SAND2008-0420C

Particle-contamination analysis for reticles in carrier inner pods

John R. Torczynski, Michael A. Gallis, Daniel J. Rader
Sandia National Laboratories, P.O. Box 5800, Albuquerque, NM, USA 87185-0346

ABSTRACT

Particle contamination is analyzed for a reticle in the inner pod of a carrier with particular emphasis on the effect of raising the cover of the inner pod before removing the reticle from the carrier at atmospheric pressure (not low pressure). Two mechanisms for particle transport into the gap between the base plate and the reticle are considered: injection and advection-diffusion. It is shown that injection is not an important mechanism but that advection-diffusion transport can carry particles deeply into the gap, where they can deposit on the reticle surface. Closed-form expressions are presented for the transmission probability that particles at the reticle edge are transported inward past the exclusion zone around the reticle perimeter. The gas flow in the gap that occurs during cover-raising is found by numerical simulation, and the closed-form expressions are applied to determine the probability of contamination for different cover-raising scenarios.

Keywords: particle, contamination, reticle, carrier, inner pod, atmospheric pressure, advection, diffusion, modeling

1. INTRODUCTION

Since contamination of the patterned surface of a reticle can impact large numbers of devices produced via lithography, protecting the reticle from particles is of interest to the semiconductor industry. One opportunity for particle contamination occurs when the inner pod of a carrier containing a reticle is opened under atmospheric pressure (see Figures 1-2).[1] As the cover is raised, particles may be produced at the contact area between the cover and the base plate and/or transported from the exterior to the interior of the inner pod by the inflow of air. Particles entering the interior have the further possibility of entering and being transported along the thin gap between the reticle and the base plate (see Figure 2) and thereby potentially depositing on the patterned surface of the reticle, which faces the base plate.

Fig. 1. Typical reticle carrier (SMIF pod): left, top view; right, bottom view. Courtesy of Geller and Rader.[2]

In this paper, the possibility that a particle travels from the edge of the reticle to the patterned region is investigated. Two particle-transport mechanisms are considered: injection and advection-diffusion. In injection, particles initially possess a large velocity relative to the air (perhaps produced during their generation) and subsequently travel a finite distance before coming to rest relative to the air. This mechanism is shown to be unimportant at atmospheric conditions. In advection-diffusion transport, particles are carried into the gap by air flow and subsequently diffuse to and deposit on solid surfaces. An approach is presented for determining the "particle transmission probability" associated with advection-diffusion transport, that is, the probability that a particle is transported from the reticle edge past the exclusion zone to the patterned surface. This approach is applied to various atmospheric-pressure cover-raising scenarios.

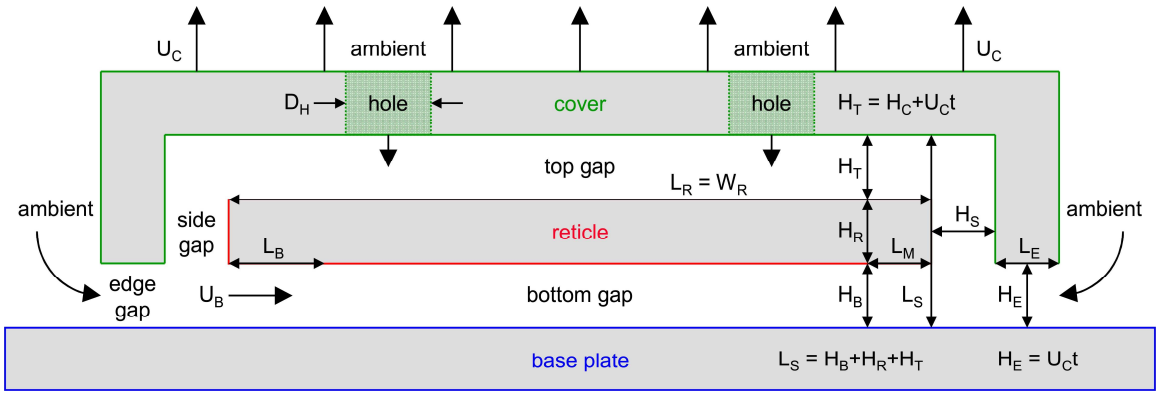

Fig. 2. Schematic diagram (not to scale) of carrier inner pod and reticle, with key geometric lengths and velocities shown.

Figure 2 shows a schematic diagram of the idealized carrier inner pod investigated herein. In this idealization, the base plate is an infinite plane without any perforations or indentations, and the cover is a square plate with rectangular edges that initially rest upon the base plate. The reticle itself is a square plate with surfaces parallel to both the base plate and the cover underside. The small posts that support a reticle in an actual inner pod are not considered here. The cover has zero or four circular holes, where each hole is centered above one quarter of the reticle. In an actual inner pod, these holes are covered by filters to prevent particle transport into the interior. The geometric lengths in Figure 2 are defined in Table 1, which provides nominal values. As the cover is raised at constant velocity, three lengths grow linearly in time: the edge gap height H_E, the top gap height H_T, and the side gap length L_S. The effects of the bottom gap height H_B, the side gap height H_S, and the cover velocity U_C on particle contamination are of particular interest.

Table 1. Geometry,[3] gas (atmospheric air),[4] and particle (PSL)[5] parameters and nominal values.

Quantity, geometry	Symbol	Value	Quantity, gas or particle	Symbol	Value
Length, reticle	L_R	152 mm	Pressure, gas	p	101325 Pa
Width, reticle	W_R	152 mm	Temperature, gas	T	300 K
Thickness, reticle	H_R	6.35 mm	Density, gas	ρ	1.177 kg/m^3
Length, exclusion zone	L_M	5 mm	Viscosity, gas	μ	0.0000185 Pa·s
Length, edge gap	L_E	5 mm	Specific heat, gas	C_p	1005 J/kg·K
Height, edge gap	H_E	$U_C t$	Thermal conductivity, gas	K	0.0261 W/m·K
Length, side gap	L_S	$H_B + H_R + H_T$	Mean free path, gas	λ	68.37 nm
Height, side gap	H_S	1-6 mm	Diameter, particle	d	10-1000 nm
Height, bottom gap	H_B	0.06-2 mm	Density, particle	ρ_s	1050 kg/m^3
Height, top gap	H_T	$H_C + U_C t$	Thermal conductivity, particle	K_s	0.08 W/m·K
Height, top gap, initial	H_C	1.31 mm	Slip correction parameter 1	α_s	1.165
Diameter, holes (four)	D_H	0-2.54 cm	Slip correction parameter 2	β_s	0.483
Velocity, cover	U_C	0.05-0.5 m/s	Slip correction parameter 3	γ_s	0.997
Velocity, flow	U_B	computed	Gravitational acceleration	g	9.81 m/s^2
Distance, flow	L_B	computed	Boltzmann constant	k_B	1.380658E−23 J/K

Several particle parameters depend on the particle diameter.[6] Formulas for these quantities are shown in Equation (1), and values for these quantities are shown in Table 2 for three particle diameters spanning the range of interest:

$$m = \frac{\pi d^3 \rho_s}{6},\ \mathrm{Kn} = \frac{2\lambda}{d},\ \beta = \frac{3\pi\mu d}{1 + \mathrm{Kn}\left(\alpha_s + \beta_s \exp\left[-\gamma_s/\mathrm{Kn}\right]\right)},$$
$$\tau = \frac{m}{\beta},\ c = \left(\frac{2k_B T}{m}\right)^{1/2},\ D = \frac{c^2\tau}{2} = \frac{k_B T}{\beta},\ \ell = \frac{\pi c \tau}{2},\ U_G = \frac{mg}{\beta}. \quad (1)$$

Table 2. Diameter-dependent particle parameters for PSL particles in atmospheric air (see Table 1).

Quantity, particle	Symbol	At $d = 10$ nm	At $d = 100$ nm	At $d = 1000$ nm
Mass	m	0.5498E−21 kg	0.5498E−18 kg	0.5498E−15 kg
Knudsen number	Kn	13.67	1.367	0.1367
Drag coefficient	β	0.7558E−13 N/(m/s)	59.88E−13 N/(m/s)	1504.E−13 N/(m/s)
Stopping time	τ	7.275 ns	91.81 ns	3656. ns
Thermal speed	c	2.190 m/s	0.06925 m/s	0.002190 m/s
Diffusivity	D	548.1E−10 m^2/s	6.917E−10 m^2/s	0.2754E−10 m^2/s
Thermal stopping distance	ℓ	25.03 nm	9.99 nm	12.58 nm
Velocity, terminal, gravity	U_G	0.7136E−07 m/s	9.006E−07 m/s	358.6E−07 m/s

A few comments about these parameters are in order. The Knudsen number indicates the importance of slip on the drag force of the air on the particle. Thus, slip is extremely important for a 10-nm particle but less so for a 1000-nm particle. The drag force is given by the product of the particle velocity relative to the air with the drag coefficient. The expression in Equation (1) for the drag coefficient correctly treats the effect of slip for all Knudsen numbers.[5-6] The stopping time is the time in which the particle velocity relative to the air is reduced by $1/e$. This quantity increases strongly with increasing particle diameter. The thermal speed represents the particle's Brownian motion that is produced by impacts from air molecules, and the diffusivity represents the spreading of particle positions that results from Brownian motion. Both of these quantities decrease strongly with increasing particle diameter. The thermal stopping distance indicates how far a particle can travel at its thermal speed during Brownian motion before changing its speed or direction significantly. The modest and nonmonotonic dependence of this quantity on particle diameter is well known[6] and occurs because of the importance of slip at small particle diameters. Diffusing particles can be roughly thought of as taking steps similar to the thermal stopping distance but in random directions. The terminal velocity results from balancing the drag and gravitational forces. This quantity is always small compared to the cover velocity (see Table 1) although it increases strongly with increasing particle diameter.

2. INJECTION PARTICLE TRANSPORT

In injection, particles initially possess a large velocity relative to the air (perhaps produced during their generation) and subsequently travel a finite distance before coming to rest relative to the air. A particle with initial velocity U_I travels a distance $L_I = U_I \tau$ before coming to rest.[6] If a 1000-nm particle with a stopping time of $\tau = 3656$ ns is injected at a speed of $U_I = 300$ m/s (roughly the speed of sound in atmospheric air[7]), it travels a distance of at most $L_I = 1$ mm (this value is actually an upper bound because the drag force on high-speed particles is even greater than predicted by the drag coefficient[7]). Other particles in the diameter range of interest have smaller stopping times, and the injection velocity considered here is unrealistically large. Since the cover edge is 1-6 mm from the reticle edge (H_S in Figure 2), particles cannot be injected into the gap under the reticle when the background gas is atmospheric air.

3. ADVECTION-DIFFUSION PARTICLE TRANSPORT

In advection-diffusion transport, particles are carried into the gap by air flow and subsequently diffuse to solid surfaces. Initially, the situation of steady air flow at mean velocity U_B in a gap of height H_B is considered (see Figure 2). Subsequently, the situation in which this air flow is maintained for a time t_B with zero air flow afterward is considered. Gravity-induced settling is ignored herein. Since settling removes particles from the air flow, this analysis provides an upper bound for the particle transmission probability along the gap and thus is conservative.

The spatial variation of the particle number density (concentration) n in the gap is described by the steady advection-diffusion equation[6] with constant fluid and particle properties, where x and y are the spatial coordinates along and across the gap (see Figure 2), $x = 0$ is the left edge of the gap, $y = \pm H_B/2$ are the upper and lower gap surfaces, and u is the x velocity component, which varies parabolically in y (appropriate for long thin gaps at modest flow speeds[8]):

$$u\frac{\partial n}{\partial x} = D\left(\frac{\partial^2 n}{\partial x^2} + \frac{\partial^2 n}{\partial y^2}\right),\ u = \frac{3}{2}U_B\left(1 - \frac{4y^2}{H_B^2}\right). \tag{2}$$

The following boundary condition applies on the upper and lower gap surfaces, where the sticking fraction s is the probability that a particle incident on a solid surface sticks to the surface ($0 \le s \le 1$):[9]

$$\mp D\frac{\partial n}{\partial y} = \frac{ncf}{\pi^{1/2}} \text{ on } y = \pm\frac{H_B}{2},\ f[s] \approx \left(\frac{s}{2-s}\right)\left(\frac{1+0.506s}{1+0.783s}\right). \tag{3}$$

As in analogous heat-transfer problems,[4] a similarity solution is sought, where k is the dimensionless decay constant, f_0 is the particle flux parameter, Pe is the Peclet number, n_0 is a constant, and $\tilde{n}$ is a function to be found:

$$n = n_0 \exp[-k\tilde{x}]\tilde{n}[k\tilde{y}],\ \tilde{x} = \frac{x}{H_B},\ \tilde{y} = \frac{y}{H_B},\ k = k[f_0, \mathrm{Pe}],\ f_0 = \frac{cH_B f}{\pi^{1/2}D},\ \mathrm{Pe} = \frac{U_B H_B}{D}. \tag{4}$$

Mathematica,[10] a computational mathematics software package, is used to find closed-form expressions for k and $\tilde{n}$. For motionless air (i.e., $\mathrm{Pe} = 0$), fairly simple expressions are obtained although the first expression must be numerically inverted to find k_0 (here, the subscript "0" denotes $\mathrm{Pe} = 0$) in terms of f_0 :

$$f_0 = k_0 \tan[k_0/2],\ \tilde{n}_0 = \cos[k_0\tilde{y}]. \tag{5}$$

For flowing air (i.e., $\mathrm{Pe} > 0$), more complicated expressions are obtained that also require numerical evaluation to find k_1 (here, the subscript "1" denotes $\mathrm{Pe} > 0$), where ${}_1\mathrm{F}_1$ is a confluent hypergeometric function:[10]

$$a = \left(\frac{3k_1\mathrm{Pe}}{2}\right)^{1/2},\ b = 1 + \frac{2k_1}{3\mathrm{Pe}},\ f_0 = a\left(1 + \frac{(ab-2)\,{}_1\mathrm{F}_1\left[\frac{5}{4} - \frac{ab}{8}, \frac{3}{2}; \frac{a}{2}\right]}{2\,{}_1\mathrm{F}_1\left[\frac{1}{4} - \frac{ab}{8}, \frac{1}{2}; \frac{a}{2}\right]}\right),$$

$$\tilde{n}_1 = {}_1\mathrm{F}_1\left[\frac{1}{4} - \frac{ab}{8}, \frac{1}{2}; 2a\tilde{y}^2\right]\exp[-a\tilde{y}^2]. \tag{6}$$

Figure 3 shows two plots of the decay constant k vs. the particle flux parameter f_0 and the Peclet number Pe. The symbols are the theoretical values from Equations (5)-(6), and the curves are easily-evaluated approximate correlations, given below, which closely match the theoretical values and have the correct limiting behavior:

$${}_1\mathrm{F}_1\left[\frac{1}{4} - \frac{a_0}{8}, \frac{1}{2}; \frac{a_0}{2}\right] = 0,\ a_0 = 3.36319,\ q_0^2 = \frac{2a_0^2}{3} = 7.54070,\ c_0 = \frac{\pi^2\left(q_0^2 + 2f_0\right)}{q_0^2\left(\pi^2 + 2f_0\right)},$$

$$k_0 \approx \left(\frac{2f_0\pi^2}{2f_0 + \pi^2}\right)^{1/2},\ k_1 \approx \left\{k_0^2 + \left(\frac{c_0\mathrm{Pe}}{2}\right)^2\right\}^{1/2} - \left(\frac{c_0\mathrm{Pe}}{2}\right). \tag{7}$$

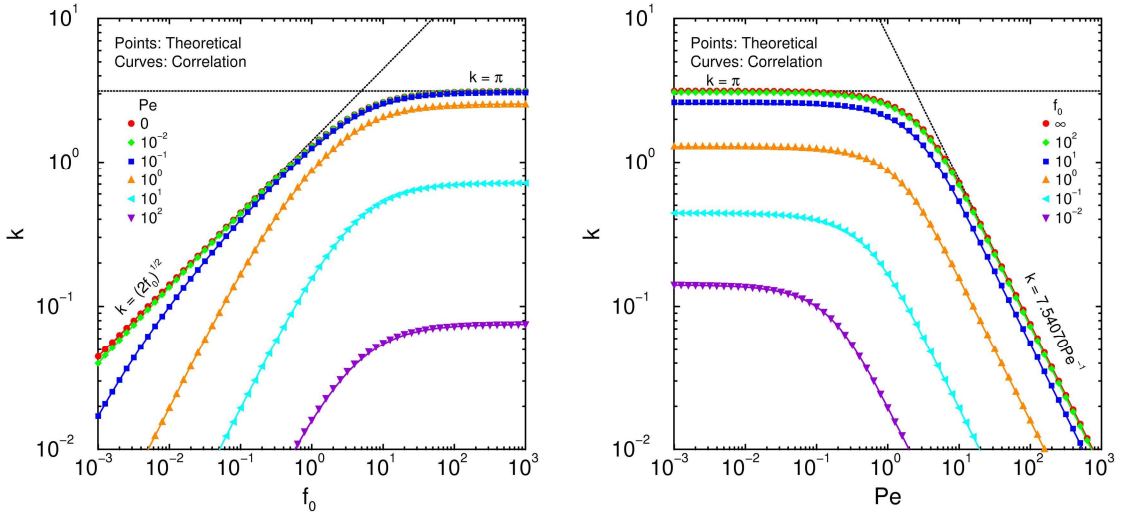

Fig. 3. Decay constant as function of particle flux parameter and Peclet number: points, theoretical; curves, correlation.

The transmission probability P that a particle released at $x = 0$ is transported beyond $x = L_M$ (past the exclusion zone, as in Figure 2) is determined by the exponential nature of the similarity solution for the particle number density n, where the decay constant is $k = k_0$ for $\mathrm{Pe} = 0$ (zero air flow) and $k = k_1$ for $\mathrm{Pe} > 0$ (nonzero air flow):

$$P = \exp[-kL_M / H_B]. \tag{8}$$

This expression can be extended to the situation of a gap of height H_B in which the air flow velocity U_B is maintained for a time t_B but is zero at later times, so that the flow travels a distance L_B and then stops (see Figure 2):

$$P = P_1 P_0,\ P_1 = \exp[-k_1 L_1 / H_B],\ P_0 = \exp[-k_0 L_0 / H_B],\ L_1 = \min\left[L_M, L_B\right],\ L_0 = L_M - L_1,\ L_B = U_B t_B. \tag{9}$$

Equation (9) is understood as arising from the application of Equation (8) first for the period with nonzero air flow and second for the period of zero air flow (denoted by the subscripts "1" and "0", respectively, as before). Equation (9) covers both the case in which the flow travels beyond the exclusion zone so that $L_B \geq L_M$ and the case in which the flow does not pass the exclusion zone so that $L_B < L_M$. In the first case, $L_1 = L_M$ and $L_0 = 0$, so $P = \exp[-k_1 L_M / H_B]$, which is simply Equation (8) for nonzero air flow. Thus, when the air flow travels beyond the exclusion zone, the air flow is considered steady because it does not matter if the air flow is terminated at some later time after the particle has already been transported beyond the exclusion zone. In the second case, $L_1 < L_M$ and $L_0 > 0$, so a particle is transported first by advection-diffusion with $\mathrm{Pe} > 0$ (i.e., nonzero flow) along a distance L_1 while its concentration decays according to k_1 and second by diffusion alone with $\mathrm{Pe} = 0$ (i.e., zero flow) along a distance L_0 while its concentration decays according to k_0. The transmission probabilities P_1 and P_0 for these two serial processes are multiplied to obtain Equation (9). In the zero-flow limit of the second case, $L_1 = 0$ and $L_0 = L_M$, so $P = \exp[-k_0 L_M / H_B]$, which is simply Equation (8) for zero air flow. Thus, Equation (9) reproduces Equation (8), which only treats strictly steady flow (either nonzero or zero), and additionally treats the situation of a flow that is steady for a finite time period and then stops.

The following five steps are followed to determine the probability of particle transmission past the exclusion zone.

1. Specify the particle thermal speed c and the particle diffusivity D, as from Equation (1) and Tables 1-2, and the gap height H_B, the exclusion zone length L_M, and the particle sticking fraction s (if unknown, use $s = 1$).
2. Specify the flow speed U_B, the flow duration t_B, and the flow distance L_B, perhaps from a flow simulation.
3. Calculate the particle flux parameter f_0 and the Peclet number Pe from Equations (3)-(4).
4. Calculate the decay constants k_0 and k_1 exactly from Equations (5)-(6) or approximately from Equation (7).
5. Calculate P, the particle transmission probability past the exclusion zone, from Equation (9).

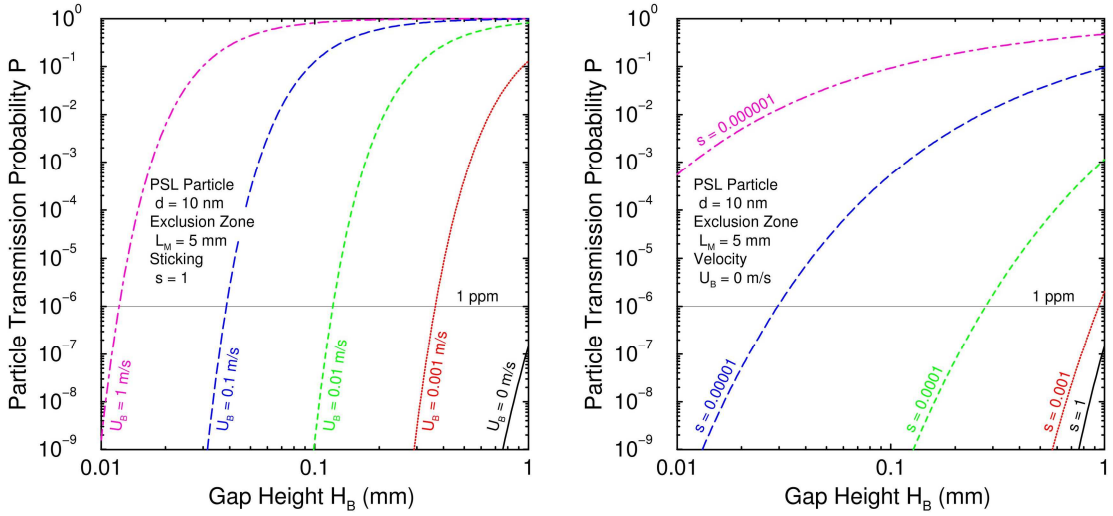

Fig. 4. Particle transmission probability as function of gap height, air flow velocity (left), and sticking fraction (right).

Figure 4 shows the transmission probability P for 10-nm PSL particles with a 5-mm exclusion zone as a function of the gap height H_B. Plots are shown for selected values of the air flow velocity U_B (here, steady, so $t_B \to \infty$) and the sticking fraction s (the probability that a particle incident on a solid surface sticks to the surface). These curves are determined from Equation (9) by applying the above five-step process. All gas and particle properties are taken from Tables 1-2, and the values for the gap height, the air flow velocity, and the sticking fraction span the ranges of interest. Results for other particle diameters are qualitatively similar. Several observations can be drawn from these results.

1. Particle transmission probability decreases strongly with decreasing gap height and can vary from essentially zero transmission to nearly unity transmission over the gap-height range of interest. Such a strong variation would appear as a "threshold" to observe contamination in an experiment.
2. Particle transmission probability increases strongly with increasing flow velocity and can become near-unity even for small flow velocities (e.g., 0.001 m/s) compared to typical cover-raising velocities (0.05-0.5 m/s). However, a flow velocity of 0.001 m/s must be maintained for 5 s to cross the 5-mm exclusion zone.
3. Particle transmission probability increases significantly with decreasing sticking fraction only when the sticking fraction becomes extremely small (e.g., $s < 0.001$, a particle sticks less than 1 time per 1000 wall impacts). Such small sticking-fraction values are unlikely to be encountered in practice.

4. CARRIER-INNER-POD COVER-RAISING APPLICATION

The five-step process developed in the previous section can be applied to determine the probability that particles are transmitted past the reticle exclusion zone when the cover of the carrier inner pod is raised under atmospheric pressure. The parameters in Step 1 are selected from the values in Tables 1-2 with the addition that the sticking fraction is set to $s = 1$ because it is unknown and does not affect the results much unless it is unrealistically small. The parameters in Step 2, namely the flow speed U_B, the flow duration t_B, and the flow distance L_B, are found from flow simulations.

The air flow that is produced when the carrier-inner-pod cover is raised has many complicated features. The flow is inherently compressible at early times despite the fact that the cover velocity and the associated flow velocities are small compared to the speed of sound, a common criterion used to indicate that compressibility can be neglected.[7] In fact, neglecting compressibility at early times produces completely erroneous results when the holes in the cover are absent. This feature prevents the use of common "incompressible-flow" simulation techniques, and the slowness of the flow velocities relative to the speed of sound also precludes the use of common "compressible-flow" simulation techniques. An even greater challenge is posed by the fact that the flow geometry changes significantly in time as the cover is raised.

One aspect of the flow geometry enables a significant simplification in the simulation of this flow. Although not obvious from Figure 2, which is not drawn to scale, the top, bottom, and edge gaps are all long and thin (i.e., their lengths are much greater than their heights, as in Table 1). With a length of $L_S \approx 8$ mm, the side gap is also long and thin when its height is $H_S = 1$ mm. At the other extreme, when its height is $H_S = 6$ mm, the side gap is an unconstricted volume, within which the pressure is spatially uniform although varying in time.

The Reynolds equation is a standard method for simulating time-varying compressible gas flows in long thin gaps that connect to unconstricted volumes.[11] For situations in which temperature variations are modest, the isothermal Reynolds equation is used, where ρ and p are the gas density and pressure, H and L are the gap height and length (both of which can vary in time and may differ from one gap to another), $\mathbf{U}$ is the average flow velocity along the gap, μ is the gas viscosity (constant for isothermal circumstances), and the subscript "0" denotes an initial value:

$$\frac{\partial}{\partial t}\left(\frac{\rho H L}{L_0}\right) + \frac{\partial}{\partial \mathbf{x}}\cdot\left(\rho H \mathbf{U}\right) = 0\,,\ \mathbf{U} = -\frac{H^2 L_0}{12\mu L}\left(\frac{\partial p}{\partial \mathbf{x}}\right),\ \frac{\rho}{\rho_0} = \frac{p}{p_0}\,. \tag{10}$$

In the Reynolds equation, the pressure, the density, and the flow velocity vary along the gap (i.e., in the flow direction) but do not vary across the gap. Therefore, the Reynolds equation involves only the two spatial coordinates along the gap: the dependent variables such as the pressure have been averaged over the third spatial coordinate across the gap.[11] This feature enables the Reynolds equation to represent a time-varying three-dimensional geometry with a time-invariant two-dimensional computational domain:[11] the averaging procedure automatically treats the time-varying gap heights. In the same spirit, the factor L/L_0 allows the time-varying side gap length to be represented on a time-invariant domain.

The Reynolds equation requires a boundary condition wherever a gap connects to the ambient external environment. This occurs in two locations, as shown in Figure 2: the entrances into the edge gap from the region outside the inner pod, and the entrances into the top gap from the cover holes if present. The following boundary condition is used to relate the pressure p and the inflow velocity U at the entrance into a gap of height H from the ambient external environment and correctly represents the limitations imposed by viscous drag and potential flow on the mass flow into the gap:[7]

$$\rho H U = 3\mu\left\{\sqrt{1 + \frac{\rho H^2\left(p_0 - p\right)}{9\mu^2}} - 1\right\}. \tag{11}$$

When gaps of different heights connect together, two quantities are continuous at the junction: the pressure p and the mass flow $\rho H U$. These conditions are applied at junctions between the following pairs of gaps (see Figure 2): top-side, bottom-side, and edge-side. The time variations of all gap heights and lengths are taken to be prescribed, as in Figure 2, wherein the top gap height H_T, the edge gap height H_E, and the side gap length L_S all grow linearly in time as the cover is raised at fixed velocity U_C.

COMSOL Multiphysics[12] is used to numerically solve Equations (10)-(11) for the inner-pod geometry of Figure 2 using the parameter values of Tables 1-2. As indicated earlier, the purpose of these flow simulations is to determine values for the flow velocity U_B, the flow duration t_B, and the flow distance L_B in the gap of height H_B between the reticle and the base plate (see Figure 2). Figure 5 shows the behavior of the pressure for representative flow simulations.

The left plot shows a typical pressure distribution in all gaps at one instant of time looking down from above the cover. The four long thin outer rectangles represent the edge gap, the four long thin middle rectangles represent the side gap (which really extends out-of-the-page but has been flattened out for presentation purposes), and the large inner square represents both the top and bottom gaps. Color-fill is used to show the pressure distribution in the edge, side, and top gaps, and contours are used to show the pressure distribution in the bottom gap (the gap of interest), which lies directly beneath the top gap. At this instant of time, the "rainbow" of color in the edge gap indicates a large pressure variation, whereas the nearly uniform blue color elsewhere indicates a rather uniform pressure distribution in the side and top gaps. The pressure in the bottom gap (shown by contours) is largest at the center and decreases toward the outer boundary.

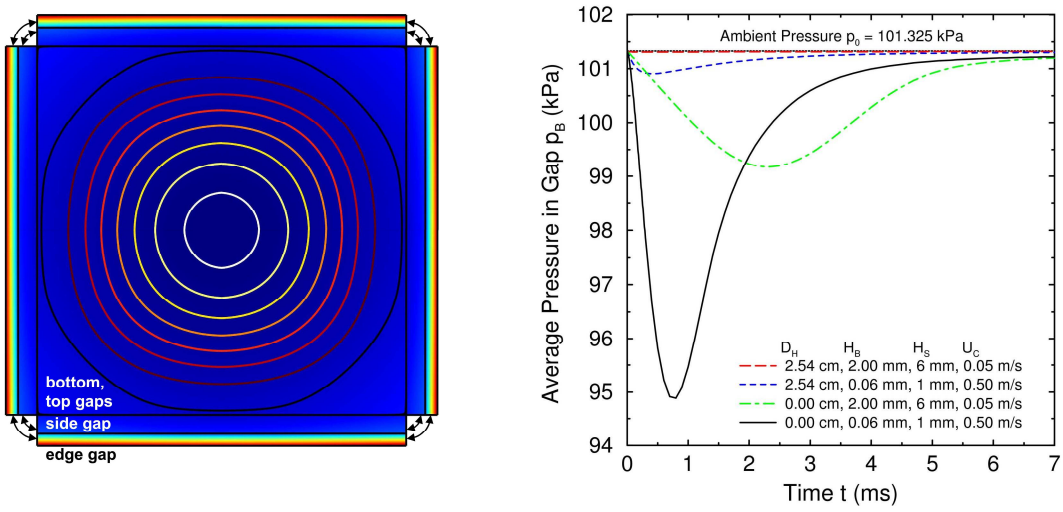

Fig. 5. Left: typical pressure distribution, shown by color-fill above and beside the reticle and contours below the reticle. Right: representative histories of average pressure in gap below reticle.

The right plot of Figure 5 shows the average pressure p_B in the bottom gap as a function of time for four cases. Two of these cases have four 2.54-cm holes in the cover, and the other two have no holes (indicated by a diameter $D_H = 0$ cm). Similarly, two of these cases have a bottom gap height of $H_B = 2.00$ mm , a side gap height of $H_S = 6$ mm , and a cover velocity of $U_C = 0.05$ m/s , whereas the other two cases have a bottom gap height of $H_B = 0.06$ mm , a side gap height of $H_S = 1$ mm , and a cover velocity of $U_C = 0.5$ m/s . The former three values lie at the extremes most likely to produce small pressure variations, whereas the latter three values lie at the extremes most likely to produce large pressure variations. Several observations can be made based on these pressure histories.

1. Pressure variations occur over 1-5 ms. Since the cover-raising velocity is 0.05-0.5 m/s, the cover rises by 1 mm or less during this time. Thus, the possibility of contamination is greatest when conditions are most uncertain.
2. The presence of holes greatly reduces pressure variations, as expected. Without holes, pressure drops can be ~6% of the ambient pressure, whereas with holes, pressure drops are well less than 1%.
3. Surprisingly, when holes are absent, varying the bottom gap height, the side gap height, and the cover velocity from one set of extremes to the other changes the pressure drop and its duration each by only a factor of 2.

Three periods of distinct flow behavior are observed for all cases.

1. Outflow. The pressure p_B decreases from its initial ambient value p_0 to its minimum value $p_B^{\min}$ at time $t_B^{\min}$, indicating that air is flowing out of the bottom gap into the side gap. Since air is flowing out of the bottom gap, particles cannot be transported inward along this gap by advection-diffusion during this period.
2. Inflow. The pressure p_B increases from its minimum value $p_B^{\min}$ at time $t_B^{\min}$ to near-ambient values by time $t \approx (2\text{-}4) t_B^{\min}$, indicating that air is flowing into the bottom gap from the side gap. Since air is flowing into the bottom gap, particles can be transported inward along this gap by advection-diffusion during this period.
3. Quiescent. The pressure p_B is near ambient and changes only slowly over much longer times, indicating that air has essentially stopped flowing into the bottom gap. Particles can still be transported inward along this gap by diffusion alone during this period.

Pressure histories of the type shown in Figure 5 can be used to determine values for the flow velocity U_B , the flow duration t_B , and the flow distance L_B in the gap of height H_B between the reticle and the base plate (see Figure 2). These values are then used in the five-step process outlined in the previous section to determine the corresponding particle transmission probability P that a particle of diameter d is transported past the exclusion zone.

As discussed above, there are three periods of distinct flow and particle-transport behavior. During the outflow period, no particles are transported into or along the bottom gap. During the inflow period, particles can be transported inward along the bottom gap by advection diffusion, and during the quiescent period, particles can be transported inward along the bottom gap by diffusion alone. Thus, the inflow period corresponds to quantities with "1" subscripts in Equation (9), and the quiescent period corresponds to quantities with "0" subscripts in Equation (9). The following definitions are used for the flow distance L_B, the flow duration t_B, and the flow velocity U_B to be used with Equation (9):

$$L_B \equiv \frac{L_R}{2}\left(1-\sqrt{\frac{p_B^{\min}}{p_0}}\right),\ t_B \equiv \int_{t_B^{\min}}^{\infty} \frac{p_0 - p_B}{p_0 - p_B^{\min}}\,dt\ ,\ U_B \equiv \frac{L_B}{t_B}\ . \tag{12}$$

The first expression is the distance that air travels back into the bottom gap as the pressure returns from its minimum value $p_B^{\min}$ to the ambient value p_0. The second expression is the time scale over which this flow occurs. The third expression is the velocity scale corresponding to this distance and this time scale.

Figure 6 shows the particle transmission probability determined using the five-step process with the above expressions for the following 144 combinations of parameter values that span the ranges of interest, along with the air and particle properties of Tables 1-2.

1. Hole diameter D_H (2 values): 0 cm (no holes, left plot), 2.54 cm (four holes, right plot).
2. Particle diameter d (3 values): 10 nm (curves), 100 nm (circles), 1000 nm (crosses).
3. Bottom gap height H_B (6 values): 0.06 mm, 0.12 mm, 0.25 mm, 0.5 mm, 1.0 mm, 2.0 mm (x-axis).
4. Cover velocity U_C (2 values): 0.50 m/s, 0.05 m/s (line type).
5. Side gap height H_S (2 values): 1 mm, 6 mm (line type).

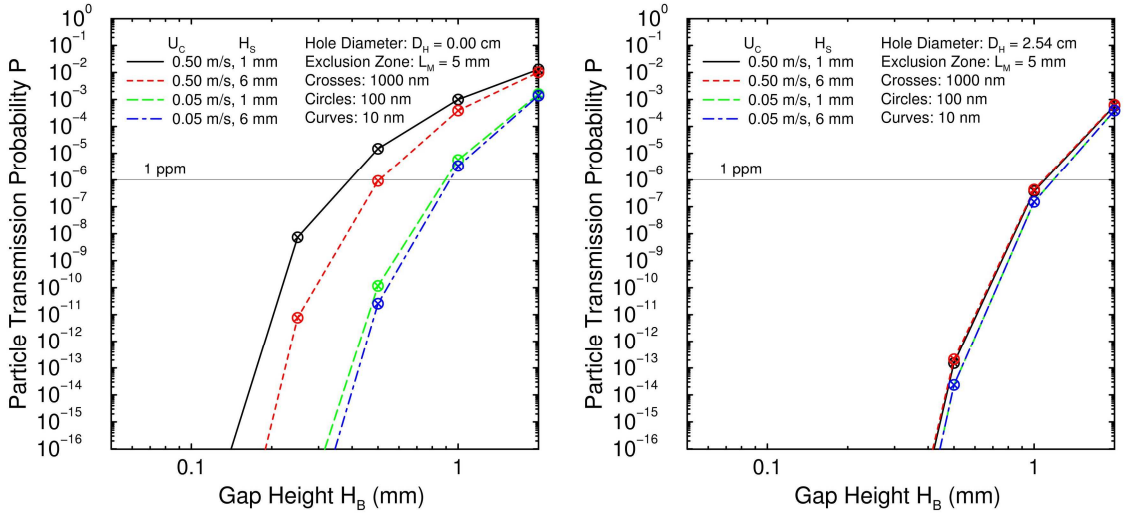

Fig. 6. Particle transmission probability vs. gap height: left; no holes in cover; right, four 2.54-cm holes in cover.

Several observations can be made about these results.

1. With all other parameters fixed, the presence of holes greatly reduces the particle transmission probability.
2. The particle transmission probability is decreased by decreasing the bottom gap height (a very strong effect), by decreasing the cover velocity (a strong effect), and by increasing the side gap height (a modest effect).
3. With all other parameters fixed, the particle transmission probability is almost independent of particle diameter over the two orders of magnitude considered.

This initially unexpected third observation can be explained in hindsight. As discussed above, there are three periods of distinct flow behavior in the bottom gap: outflow, in which no particles are transmitted; inflow, in which particles are transported by advection-diffusion; and quiescent, in which particles are transported by diffusion alone. In all cases examined, the flow distance L_B is less than the exclusion zone length L_M, and the flow velocity U_B is fast enough to ensure near-unity transmission over the distance $L_1 = L_B$. Under these circumstances, the particle transmission probability is given approximately by $P \approx \exp\left[-k_0 \left(L_M - L_B\right)/H_B\right]$. The exclusion zone length L_M and the bottom gap height H_B are geometric parameters and thus do not depend on the particle diameter. Similarly, the flow distance L_B is determined by the flow and does not depend on the particle diameter. The zero-flow particle decay constant k_0 depends on the particle flux parameter f_0, which depends on both the particle thermal speed c and the particle diffusivity D, both of which depend strongly on the particle diameter. However, for all parameter combinations considered herein, $f_0 > 1000$, so $k_0 \approx \pi$ (see the left plot of Figure 3) and therefore does not vary significantly with the particle diameter. In fact, the simple formula $P \approx \exp\left[-\pi \left(L_M - L_B\right)/H_B\right]$ reproduces all values in Figure 6 to within a factor of 2.

Two final comments are in order. First, the neglect of gravity is seen to be reasonable since particles settle well less than their diameters during the 5 ms or less in which there is significant air flow (see the right plot in Figure 5). Second, any cover-raising scenario that produces a flow distance L_B that exceeds the exclusion zone length L_M is likely to produce contamination because the particle transmission probability for the inflow period is near unity, as discussed above.

5. CONCLUSIONS

Particle contamination is analyzed for a reticle in a carrier inner pod when its cover is raised at atmospheric pressure. Injection cannot transport particles from the cover edge into the bottom gap between the reticle and the base plate: even large high-speed particles stop rapidly and cannot travel from the cover and to the reticle. Advection-diffusion transport (i.e., inward air flow plus random particle motion) can carry particles into the bottom gap. Closed-form expressions are developed for the particle transmission probability, the probability that a specified flow can transport a particle from the entrance of the bottom gap past the exclusion zone, beyond which it can deposit on the reticle. Flow simulations are performed for a wide range of cover-raising scenarios to find the flow parameters used in these closed-form expressions. For all cases, the particle transmission probability is almost independent of particle diameter over the range 10-1000 nm. An explanation is given for this unexpected result. As expected, the presence of holes in the cover greatly reduces the pressure departures from ambient and the associated air flows and thereby greatly reduces the likelihood of contamination. For typical cover-raising scenarios, the particle transmission probability becomes near-unity whenever the flow distance in the bottom gap (the product of its velocity and its duration) exceeds the exclusion zone length.

Future efforts to assess particle contamination of reticles in carrier inner pods should focus on the following areas.

1. Reticle lift. In many simulations (especially those without holes), the pressure difference from the bottom gap to the top gap greatly exceeds the value required to balance gravity and lift the reticle. However, the duration of this pressure difference is short. The coupled dynamic response of the reticle and the gas should be studied.
2. Cover lowering. When the cover is lowered, the pressure in the inner pod exceeds the ambient value for some period, which produces an air flow into the bottom gap that can transport particles by advection-diffusion. Subsequently, the pressure relaxes to ambient, which produces an outward air flow. The particle transmission probability should be determined for realistic cover-lowering scenarios.
3. Low pressure. This study is focused on atmospheric conditions. At low pressures, the phenomenon of slip can change many behaviors quantitatively and perhaps qualitatively. For example, injected particles travel farther, all particles settle faster, and gases flow more easily. The techniques developed and applied herein should be extended and applied to low-pressure situations.
4. Pumping and filling. Pressure changes caused by pumping from ambient to vacuum and by filling from vacuum to ambient produce a variety of flows that can transport particles. Moreover, these flows are nonisothermal, so thermophoretic forces can induce particle motion as well. These situations should be studied.

6. ACKNOWLEDGMENTS

This work was performed at Sandia National Laboratories. Sandia is a multiprogram laboratory operated by Sandia Corporation, a Lockheed Martin Company, for the United States Department of Energy's National Nuclear Security Administration under contract DE-AC04-94AL85000. The authors gratefully acknowledge financial support from Intel Corporation under CRADA SC93/01154 and technical interactions with Kevin J. Orvek, Intel contract monitor, Long He, SEMATECH, David Y.-H. Pui and his students, University of Minnesota, and Christof Asbach and Heinz Fissan, IUTA, Deutschland.

REFERENCES

1. M. Sogard, "EUV Reticle Carrier—Joint Proposal and Current Status of Canon and Nikon," SEMICON West 2005, San Francisco, CA, July 12-14, 2005.
2. A. S. Geller and D. J. Rader, "Improved Reticle Carrier Design through Numerical Simulation," EUV Mask Standards Workshop, San Jose, CA, February 28, 2005.
3. K. J. Orvek, Intel Corporation (private communication), 2007.
4. F. M. White, *Heat Transfer*, Addison-Wesley Publishing Company, Reading, MA, 1984.
5. J. H. Kim, G. W. Mulholland, S. R. Kukuck, and D. Y. H. Pui, "Slip Correction Measurements of Certified PSL Nanoparticles Using a Nanometer Differential Mobility Analyzer (Nano-DMA) for Knudsen Number from 0.5 to 83," *Journal of Research of the National Institute of Standards and Technology*, 110(1), 31-54 (2005).
6. S. K. Friedlander, *Smoke, Dust, and Haze: Fundamentals of Aerosol Dynamics*, Oxford University Press, New York, NY, 2000.
7. P. K. Kundu and I. M. Cohen, *Fluid Mechanics*, 3rd Ed., Elsevier Academic Press, Amsterdam, Netherlands, 2004.
8. F. M. White, *Viscous Fluid Flow*, McGraw-Hill Book Company, New York, NY, 1974.
9. M. A. Gallis, J. R. Torczynski, and D. J. Rader, "Nanoparticle Knudsen Layers in Gas-Filled Microscale Geometries," *Physical Review E*, submitted (2008).
10. S. Wolfram, *The Mathematica Book*, 5th Edition, Wolfram Media, Champaign, IL, 2003.
11. G. E. Karniadakis and A. Beskok, *Micro Flows: Fundamentals and Simulation*, Springer-Verlag, New York, NY, 2002.
12. COMSOL AB, *COMSOL Multiphysics User's Guide*, Version 3.3, COMSOL AB, Stockholm, Sweden, 2006.